Rapid Communications

Reconfigurable topological states in valley photonic crystals

You Wu,[1] Xiaoyong Hu,[1,2,*] and Qihuang Gong[1,2]

[1]*State Key Laboratory for Mesoscopic Physics, Department of Physics, Collaborative Innovation Center of Quantum Matter, Peking University, Beijing 100871, China*

[2]*Collaborative Innovation Center of Extreme Optics, Shanxi University, Taiyuan, Shanxi 030006, China*

(Received 4 August 2018; published 21 December 2018)

Valley photonic crystals can enable nontrivial topology locked to the valley index. Since time-reversal symmetry is preserved, no external magnetic field has to be applied. Therefore, the valley topological insulators can be easily used to construct photonic devices. Here, a reconfigurable valley photonic crystal is proposed, where the inversion symmetry is broken by constructing the unit cell with two different materials. Also, since one of the materials is electro-optic material barium titanate, by simply changing the applied voltage, not only the band-gap frequency will shift, but the topological phase transition can also happen. This is highly beneficial to the design and optimization of integrated photonic devices because a balance between the flexibility of devices and the robustness of topological properties is realized successfully. Moreover, a two-port optical switch as an example of the possible applications is proposed.

DOI: 10.1103/PhysRevMaterials.2.122201

I. INTRODUCTION

Semiconductor technologies and traditional electronics are mainly based on the use of the electronic charge. However, spin and valley are another two degrees of freedom that could be utilized to carry and process information. In addition to the spintronics, valleytronics has also been developing rapidly in recent years [1–8]. Valley is the energy extrema of bands in reciprocal space. In some two-dimensional materials, the breaking of inversion symmetry can lead to the optical selection rules, so that valley-dependent electronic activities can be realized with light incidence of different circular polarizations [5–8]. Recently, the valley degree of freedom was also introduced to photonics [9–18], and the so-called valley photonic crystals were investigated both theoretically and experimentally, where nontrivial topological states were observed [16–18]. In the past decade, the concept of topology was introduced to photonics [19–21]. Photonic topological insulators were predicted and experimentally discovered in lots of photonic systems [15,18,22–31], similar to the quantum Hall effect or quantum spin Hall effect. Owing to the unique property of topological protection, edge states between two topologically distinct photonic materials can propagate unidirectionally without backscattering. Topological photonics has then been an emerging field of research and is believed to bring about breakthroughs in both fundamental physics and integrated photonic devices [32].

In quantum spin Hall effect, two edge states propagate in opposite directions, which are locked to their spin. Similarly, in valley photonic crystals, there are also two edge states propagating in opposite directions, while they are locked to the valley degree of freedom. Besides, these edge states are protected against many kinds of defects as long as they will not lead to intervalley scattering. Compared with the quantum Hall effect systems where time-reversal symmetry is broken, valley photonic topological insulators do not need external magnetic field, while the inversion symmetry has to be broken instead. Therefore, valley photonic topological insulators are more likely to be realized at visible or near-infrared frequencies. Usually, to break the inversion symmetry, the geometry in a unit cell has to be designed specially, such as making the radii of the two rods in a unit cell different [9], modifying the circular rod in a honeycomb cell to a triangular prism [12], changing the orientation of Y-shaped rods [14], or detuning the refractive index of the two honeycomb sublattices [18]. However, all these structures cannot be tuned actively, which is a drawback when considering future applications. In microwave region, reconfigurable photonic topological insulators can be realized by moving the collars with motorized arms [30]. However, at visible or near-infrared wavelengths, it is much more challenging to realize active control of the topological states. One recent study proposed a possible concept where liquid crystals were introduced as the background material, so that the topological band gap will be shifted with different applied voltages [13]. Another similar study was based on graphene, whose chemical potential is tunable with external bias voltage, so that the effective refractive index can be effectively tuned [33]. Nevertheless, in these systems topological phase transition still cannot be realized. Technically speaking, reconfigurability and robustness of the edge states are contradictory to some extent because of the topological protection.

Here, we proposed a reconfigurable valley photonic crystal, which enables dynamic control of its topological property. By tuning the refractive index of one rod in each unit cell, the inversion symmetry is broken, leading to nontrivial topology locked to each valley. Furthermore, the topological phase transition can happen in the band gap, so that the control of the topological edge states is possible. This structure can be

*xiaoyonghu@pku.edu.cn

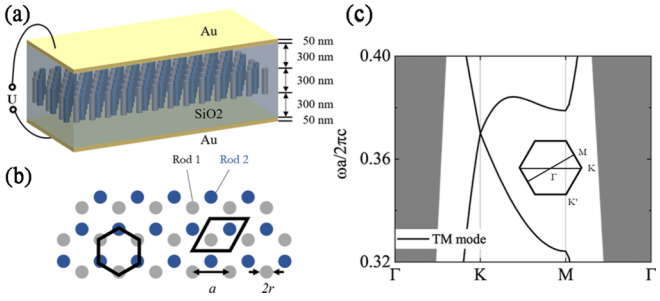

FIG. 1. (a) Three-dimensional configuration of the reconfigurable valley photonic crystal. The photonic crystal rod slab is embedded in a SiO_2 layer, and covered by two gold films on the top and bottom. (b) A two-dimensional model of the valley photonic crystal composed of TiO_2 (rod 1, gray rods) and $BaTiO_3$ (rod 2, blue rods). The black hexagon and rhombus are primitive cells including two rods. The lattice constant is a, and the rod's radius $r = 3\sqrt{3}/25a$. The background material is air ($n_0 = 1$). (c) The band structure of the TM mode for the two-dimensional photonic crystals when $n_{TiO_2} = n_{BTO}$ (the gray area is the light cone). There exists a Dirac cone at the K (K') point. The inset is the first Brillouin zone.

used to construct complex integrated photonic devices, which can operate at optical communication wavelengths, taking advantage of its tunability of topological properties.

II. RECONFIGURABLE VALLEY PHOTONIC TOPOLOGICAL INSULATORS

The three-dimensional configuration is shown in Fig. 1(a). The photonic crystal rod slab is 300 nm in thickness, and is embedded in the center of a SiO_2 layer with the thickness of 900 nm. The whole structure is covered by two gold films on the top and bottom, which can effectively restrict the leak of the field to the free space and improve the transmittance [34]. This three-dimensional model can be reduced to two dimensions, according to the method of effective index approximation [35,36]. In this work, since we have to continuously tune the refractive index of $BaTiO_3$ rods, a direct two-dimensional approximation was used for the simplification, as shown in Fig. 1(b). The refractive indexes of the rods are considered the same as those in three dimensions, while the background material is considered as air here. This may lead to the shift of band structures, while the topological properties of this structure are preserved since the symmetry remains unchanged, and more details can be found in the Supplemental Material [37]. Here, the two-dimensional photonic crystal has a honeycomb lattice, which contains two rods in a rhombus unit cell, as illustrated in Fig. 1(b). The materials of the rods are TiO_2 and $BaTiO_3$, respectively, whose refractive indices are both 2.38 around 1550 nm [38,39]. Due to the C_{6v} symmetry of this honeycomb structure, Dirac cones will emerge at K or K' points in the first Brillouin zone. The band structure for the TM mode is shown in Fig. 1(c), where the out-of-plane E_z and in-plane H_x and H_y are nonzero. The Dirac degeneracy is often a critical point where topological phase transition happens. In order to open a band gap, either time-reversal symmetry or inversion symmetry has to be broken. In this work, the inversion symmetry is broken by tuning the refractive index of $BaTiO_3$, which can be regarded as different onsite energies at two rods from the view of condensed matter physics [18].

$BaTiO_3$ is a linear electro-optic material, whose refractive index is tunable with applied external electric field according to the Pockels effect. $BaTiO_3$ has one of the largest effective electro-optic coefficients, and we assume $r_{eo} = 210$ pm/V [39,40]. Therefore, the refractive index of $BaTiO_3$ has the form of

$$n_{BTO} = n + \frac{1}{2} r_{eo} n^3 \frac{U}{L}. \tag{1}$$

Here, n_{BTO} can be continuously tuned from 2.26 to 2.5, with $n = 2.38$ and the distance between two electrodes $L = 900$ nm, if the voltage U is tuned from -75 to 75 V. The electric field strength is 8.3×10^7 V/m, which is below the breakdown strength of $BaTiO_3$ [41–43], and this refractive index change is reasonable [44].

As shown in Fig. 2(a), we calculated the first two bands of the two-dimensional valley photonic crystal, when n_{BTO} equals 2.26 and 2.5. There is a red-shift of the band gap with the increase of n_{BTO}. The band gap ranges from $0.3710 \times 2\pi c/a$ to $0.3857 \times 2\pi c/a$ when $n_{BTO} = 2.26$, and from $0.3553 \times 2\pi c/a$ to $0.3690 \times 2\pi c/a$ when $n_{BTO} = 2.5$. Furthermore, we focus on the eigenstates at K and K' valleys of the first two bands. The phase distribution of E_z component and Poynting vectors (black arrows) are shown in Fig. 2(b). By defining a topological charge as $l = \oint_L \nabla[\arg(E_z)]d\vec{s}/2\pi$, where the integration is along a closed path surrounding the phase singularity, the eigenstates can be classified as either right-handed circular polarized (RCP, $l = 1$) or left-handed circular polarized (LCP, $l = -1$) orbital angular momentum at the K (K') point [9,45]. When $n_{BTO} = 2.26$, the phase distribution indicates a RCP orbital angular momentum at K point and a LCP orbital angular momentum at K' point for the first band. For the second band, the eigenstates are LCP and RCP at the K point and K' point, respectively. However, when n_{BTO} is increased to 2.5, which is larger than n_{TiO_2}, the eigenstates of each band at the K (K') valleys will be interchanged, accompanied with the red-shift of the band gap. Under this circumstance, the eigenstate of the first band is LCP (RCP) at K (K') point, while it is RCP (LCP) at K (K') point for the second band. This interchange of the eigenstates indicates that band inversion happens in this process, which is also a direct evidence of topological phase transition. On the other hand, the effective Hamiltonian is [9]

$$\hat{H} = v_D(\hat{\sigma}_x \hat{\tau}_z \delta k_x + \hat{\sigma}_y \delta k_y) + \lambda \hat{\sigma}_z, \tag{2}$$

where $\delta \boldsymbol{k}$ is the vector from K or K' valley in the reciprocal space, and $\hat{\sigma}_i$, $\hat{\tau}_i$ are Pauli matrices. $\lambda \propto (\int_1 \varepsilon_1 ds - \int_2 \varepsilon_2 ds)$, and it is either positive or negative based on whether n_{BTO} is smaller or larger than n_{TiO_2}. For example, λ is positive when $n_{BTO} = 2.26$, while it is negative when $n_{BTO} = 2.5$. Although there exist band gaps either when $\lambda > 0$ or $\lambda < 0$, the topological properties are different. According to the definition of Chern number [46], the valley-Chern index can be written as [12]

$$C^{(v)} = \frac{1}{2\pi} \iint_{BZ(v)} \nabla_{\boldsymbol{k}} \times \langle u(\boldsymbol{k}) | i \nabla_{\boldsymbol{k}} | u(\boldsymbol{k}) \rangle \cdot d\boldsymbol{s}, \tag{3}$$

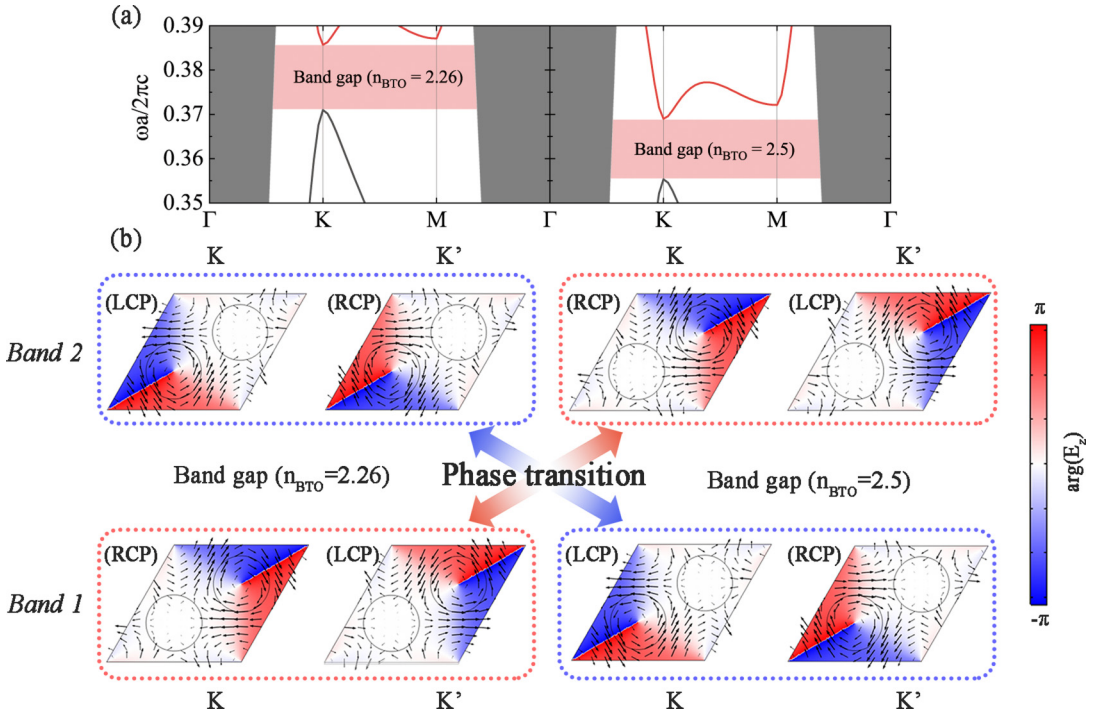

FIG. 2. Topological phase transition along with band inversion. (a) A band gap (pink shaded area) emerges as long as $n_{\mathrm{BTO}} \neq n_{\mathrm{TiO_2}}$. The band gap is from $0.3710 \times 2\pi c/a$ to $0.3857 \times 2\pi c/a$ when $n_{\mathrm{BTO}} = 2.26$, and from $0.3553 \times 2\pi c/a$ to $0.3690 \times 2\pi c/a$ when $n_{\mathrm{BTO}} = 2.5$. (b) The eigenstates (phase profile of E_z component) at K and K' for bands 1 and 2 when $n_{\mathrm{BTO}} = 2.26$ and 2.5, respectively. The black arrows represent the direction of Poynting vectors. The eigenstates of bands 1 and 2 are inversed in the process when n_{BTO} increases from 2.26 to 2.5, indicating the topological phase transition at the critical point when $n_{\mathrm{BTO}} = n_{\mathrm{TiO_2}}$. The orbital angular momentum of each state is marked in the parentheses on the top left of each panel: left circular polarization (LCP) or right circular polarization (RCP).

where v labels the valley, the integral region is half of the first Brillouin zone, and $u(\boldsymbol{k})$ is the spatially periodic part of the Bloch function. Taking use of the numerical simulation results, $C^{(v)}$ can be obtained directly. Here, based on the effective Hamiltonian, the valley Chern indices can also be simply calculated according to the sign of λ:

$$C^{(K,K')} = \pm\tfrac{1}{2}\mathrm{sgn}(\lambda). \tag{4}$$

Therefore, when $n_{\mathrm{BTO}} < n_{\mathrm{TiO_2}}$, $C^{(K)} = 1/2$ and $C^{(K')} = -1/2$; when $n_{\mathrm{BTO}} > n_{\mathrm{TiO_2}}$, $C^{(K)} = -1/2$ and $C^{(K')} = 1/2$. The topological invariant is then defined as $C_v = C^{(K)} - C^{(K')}$, and $C_v = 1$ (-1) when $n_{\mathrm{BTO}} < n_{\mathrm{TiO_2}}$ $(n_{\mathrm{BTO}} > n_{\mathrm{TiO_2}})$, respectively. This verifies the topological phase transition as well.

III. VALLEY-DEPENDENT TOPOLOGICAL EDGE STATES

When two valley photonic crystals with distinct valley Chern numbers are spliced, valley-dependent topological edge states are supported. As shown in Figs. 3(a) and 3(c), two types of edge can be constructed, respectively. Here, we assume $n_{\mathrm{BTO}} = 2.26$. Taking Fig. 3(a) as an example, C_v equals 1 for the upper photonic crystal. As for the lower photonic crystal, the unit cell can be regarded as the same of the upper photonic crystal, except that it is rotated by 180°. Therefore, the first Brillouin zone is also rotated by 180°, so that the K valley and K' valley are interchanged. As a result, C_v is -1 for the lower photonic crystal, and the topological properties on the two sides of the edge are different. Consequently, there will exist one interfacial mode in the band gap for each valley, according to bulk-boundary correspondence [47]. Figures 3(b) and 3(d) are the corresponding energy density profiles for the two types of edge, respectively ($\omega = 0.3756 \times 2\pi c/a$), where the electromagnetic field is confined at the edge. Figure 3(e) is the dispersion curve of edge states, where the blue and red curves correspond to edge types 1 and 2, respectively. Obviously, the edge states propagate unidirectionally at each valley. These are also called valley-dependent topological edge states, and these edge states are protected from some defects or sharp bending. Different from the well-known quantum Hall effect, where the nonzero Chern number ensures the gapless unidirectional edge states due to the break of time-reversal symmetry [20], in this system the Chern number is zero and time-reversal symmetry is preserved. However, the valley-dependent edge states are still robust, as long as there is no intervalley scattering. Figure 4(a) is the transmittance for four different structures, which are a bulk photonic crystal without an edge (black solid line), a Z-shape edge (red dashed line), a type 1 straight edge (blue dotted line), and a type 2 straight edge (green dashed-dotted line). It is distinct that for the bulk structure, the transmittance is close to zero in the band gap (pink area), while for the topological edges, the transmittance is over 80% whether there is a sharp bending or not. Figure 4(b) shows the energy density profile of an edge state propagating through a Z-shape bending. Most of the electromagnetic energy propagates through the bending without backscattering. More calculation results about the

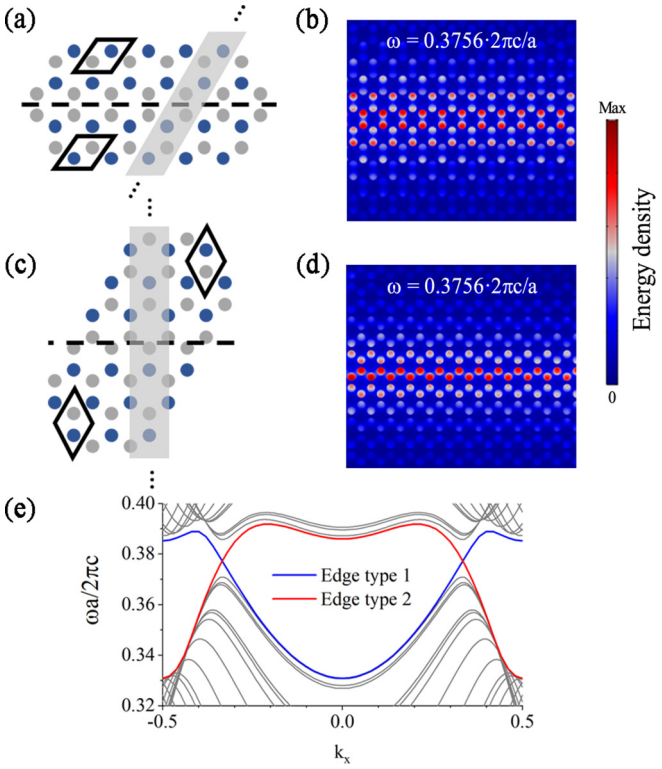

FIG. 3. Valley-dependent topological edge states. Panels (a) and (c) are two types of edge, constructed by valley photonic crystals with different topological properties. Panels (b) and (d) are corresponding energy density distribution at the frequency of $0.3756 \times 2\pi c/a$. (e) The blue and red lines are the calculated dispersion curves for edge types 1 and 2, respectively, and the gray lines are bulk states.

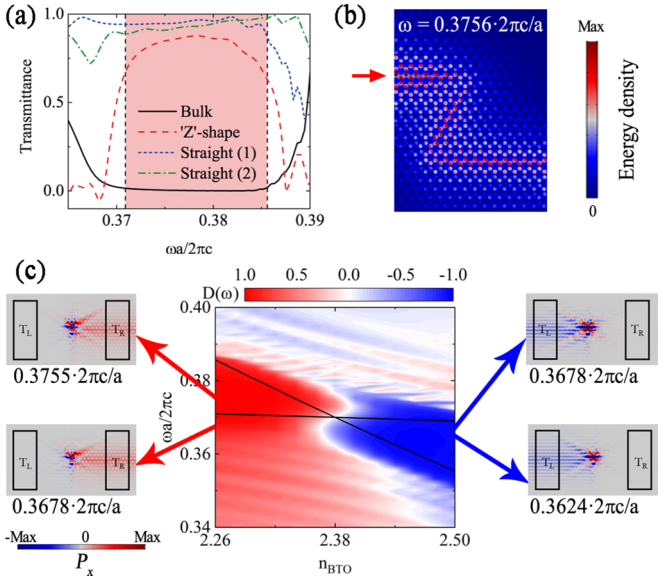

FIG. 4. (a) The transmittance curves of a bulk photonic crystal (black solid line), a Z-shape edge (red dashed line), a type 1 straight edge (blue dotted line), and a type 2 straight edge (green dashed-dotted line). The pink area is the band gap. (b) The energy density profile at $0.3756 \times 2\pi c/a$ for the Z-shape bending when light is input from the left port (red arrow). (c) The directionality $D(\omega)$ under different n_{BTO}. $D(\omega)$ is close to either 1 or -1 in the band gap indicated by the two black lines when $n_{\mathrm{BTO}} < n_{\mathrm{TiO_2}}$ or $n_{\mathrm{BTO}} > n_{\mathrm{TiO_2}}$, respectively. The insets are the P_x component at $0.3678 \times 2\pi c/a$ and $0.3755 \times 2\pi c/a$ when $n_{\mathrm{BTO}} = 2.26$, and at $0.3624 \times 2\pi c/a$ and $0.3678 \times 2\pi c/a$ when $n_{\mathrm{BTO}} = 2.5$, respectively.

robustness against defects can be found in the Supplemental Material [37].

In order to further investigate the directionality of the valley-dependent topological edge states quantificationally, we plot the directionality $D(\omega)$ of edge type 2 when $n_{\mathrm{BTO}} = 2.26$ in Fig. 4(c), which is defined as

$$D(\omega) = \frac{T_R(\omega) - T_L(\omega)}{T_R(\omega) + T_L(\omega)}. \tag{5}$$

Here, T_L and T_R are the integral of x component of Poynting vector: $T_i = \int_i P_x dx\, dy$, $i = L, R$. The integral area is a rectangular sized $6a \times 15a$, and is $12a$ away from the excitation source. The unidirectionally propagating edge states are launched by two perpendicular dipoles with the same amplitude and a phase difference of $\pm\pi/2$, for example, $\boldsymbol{H} = H_0(\vec{x} \pm i\vec{y})$. This is due to the propagating direction of the valley topological edge states are locked to the circular polarized orbital angular momentum [9,14,48]. The polarization selective excitation of directional propagating modes was observed in many optical systems recently [49–53]. From Fig. 4(c), it is clear that edge states in the band gap propagate unidirectionally, and $D(\omega) \approx \pm 1$. Here, the two black lines indicate the boundaries of the band gap between the first two bands. It also agrees well with the topological phase transition we discussed before. The x component of Poynting vector at $0.3678 \times 2\pi c/a$ and $0.3755 \times 2\pi c/a$ when $n_{\mathrm{BTO}} = 2.26$, and at $0.3624 \times 2\pi c/a$ and $0.3678 \times 2\pi c/a$ when $n_{\mathrm{BTO}} = 2.5$ are shown in the insets. It can be easily found that the edge modes propagate unidirectionally and are confined well beside the edge.

IV. APPLICATION: TWO-PORT OPTICAL SWITCH

Owing to the unique properties of topological photonic crystals, optical signals can be easily controlled in these structures and lots of new photonic devices have been proposed and realized [32]. If combined with reconfigurability of topological states, these devices are expected to be much more flexible and some new devices can be developed.

As an example, we present a possible application of a two-port optical switch here. As depicted in Fig. 5(a), the two-port switch is simply constructed by two topologically distinct valley photonic crystals. The parameters are the same as those in Fig. 1, and there is a type 2 edge in the center. A circularly polarized source of $\boldsymbol{H} = H_0(\vec{x} - i\vec{y})$ is located at one rod near the edge [red star in Fig. 5(a)], which can selectively excite one of the edge states in a certain valley, according to the analysis before. Figure 5(b) shows the dispersion curve when n_{BTO} equals 2.26 and 2.5, respectively. For each valley, the propagation direction is reversed due to the topological phase transition. For example, first the voltage is -75 V ($n_{\mathrm{BTO}} = 2.26$), and therefore the edge states mostly propagate through the right port in the band gap. When the voltage is switched to 75 V ($n_{\mathrm{BTO}} = 2.5$), the edge states will propagate towards the left side in the band gap instead. The results are

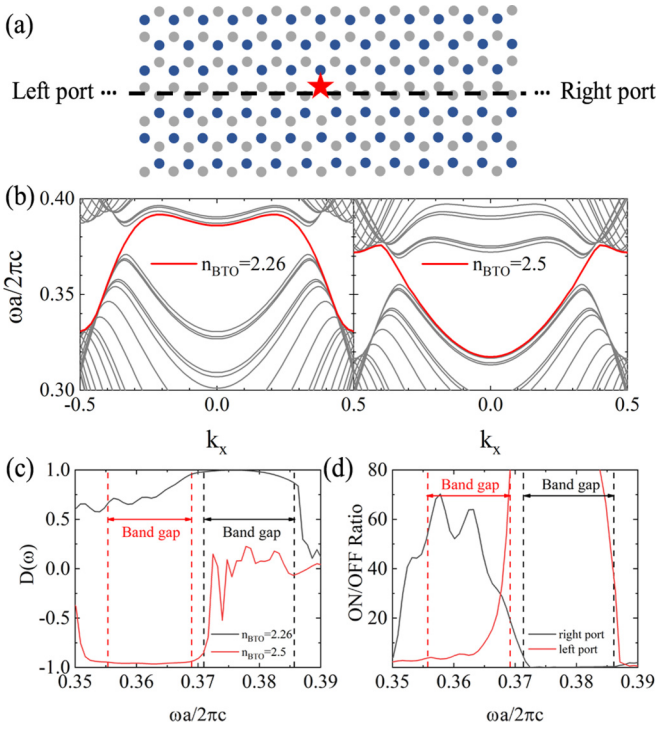

FIG. 5. A two-port optical switch based on valley photonic crystals. (a) The structure of the optical switch, where an edge is formed by two topologically distinct valley photonic crystals. A circularly polarized dipole [$\boldsymbol{H} = H_0(\vec{x} - i\vec{y})$, marked as a red star] excites the topological edge states, and the edge states will propagate through either the left port or the right port. (b) The dispersion curves of the edge states when $n_{\mathrm{BTO}} = 2.26$ or 2.5, respectively. (c) The directionality $D(\omega)$ is close to 1 or -1 in the band gap. (d) The ON/OFF ratio of this optical switch for both ports.

plotted in Fig. 5(c), where we can find that $D(\omega)$ is either close to 1 or -1 in the band gap based on n_{BTO}. Therefore, by changing the sign of the applied voltage, the two ports can be switched to ON or OFF states. In order to confirm the performance of this optical switch, ON/OFF ratios for each port are calculated and shown in Fig. 5(d), which are defined as $T^i_{\mathrm{ON}}/T^i_{\mathrm{OFF}}$ ($i = 2.26, 2.5$). Here, the calculation of T^i_{ON} and T^i_{OFF} are similar as that of T_R and T_L in Eq. (5). In the band gap, the maximum of the ratio can be larger than 14 000. Here. we can choose a working frequency of $\omega = 0.3678a/2\pi c$, where $D > 92\%$ for both ports and the ON/OFF ratio is 32.8 (28.9) for the left (right) port. Therefore, the two-port optical switch we propose here not only has very high performance, but can also tolerate some defects or impurities due to the topological protection.

V. SUMMARY

In conclusion. we proposed a reconfigurable valley photonic crystal composed of TiO_2 and electro-optic material $BaTiO_3$. By tuning the external voltage, the refractive index of $BaTiO_3$ will be changed either larger or smaller than that of TiO_2, so that the inversion symmetry is broken and nonzero valley Chern number is obtained. Moreover, we verified that band inversion can happen in this photonic system and topological phase transition can be realized. Valley-dependent topological edge states are also studied in simulations, and they can propagate unidirectionally through sharp bending without backscattering. This work addressed the contradiction between the robustness of topological protection and the need of flexibility in applications. This reconfigurable valley photonic crystal is expected to be realized experimentally at optical communication frequencies, and brings about breakthroughs in integrated photonic devices.

ACKNOWLEDGMENTS

This work was supported by the 973 Program of China under Grant No. 2014CB921003, and the National Natural Science Foundation of China under Grants No. 11734001, No. 61775003, No. 61475003, and No. 11527901.

[1] L. Ju, Z. Shi, N. Nair, Y. Lv, C. Jin, J. Velasco, J., C. Ojeda-Aristizabal, H. A. Bechtel, M. C. Martin, A. Zettl, J. Analytis, and F. Wang, Nature (London) **520**, 650 (2015).
[2] D. Xiao, G. B. Liu, W. Feng, X. Xu, and W. Yao, Phys. Rev. Lett. **108**, 196802 (2012).
[3] D. Xiao, W. Yao, and Q. Niu, Phys. Rev. Lett. **99**, 236809 (2007).
[4] B. Zhu, H. Zeng, J. Dai, Z. Gong, and X. Cui, Proc. Natl. Acad. Sci. USA **111**, 11606 (2014).
[5] K. F. Mak, K. He, J. Shan, and T. F. Heinz, Nat. Nanotechnol. **7**, 494 (2012).
[6] J. R. Schaibley, H. Yu, G. Clark, P. Rivera, J. S. Ross, K. L. Seyler, W. Yao, and X. Xu, Nat. Rev. Mater. **1**, 16055 (2016).
[7] Z. Sun, J. Gu, A. Ghazaryan, Z. Shotan, C. R. Considine, M. Dollar, B. Chakraborty, X. Liu, P. Ghaemi, S. Kéna-Cohen, and V. M. Menon, Nat. Photonics **11**, 491 (2017).
[8] H. Zeng, J. Dai, W. Yao, D. Xiao, and X. Cui, Nat. Nanotechnol. **7**, 490 (2012).
[9] X.-D. Chen, F.-L. Zhao, M. Chen, and J.-W. Dong, Phys. Rev. B **96**, 020202(R) (2017).
[10] J.-J. Chen, S.-Y. Huo, Z.-G. Geng, H.-B. Huang, and X.-F. Zhu, AIP Adv. **7**, 115215 (2017).
[11] J. W. Dong, X. D. Chen, H. Zhu, Y. Wang, and X. Zhang, Nat. Mater. **16**, 298 (2017).
[12] T. Ma and G. Shvets, New J. Phys. **18**, 025012 (2016).
[13] M. I. Shalaev, S. Desnavi, W. Walasik, and N. M. Litchinitser, New J. Phys. **20**, 023040 (2018).
[14] L. Ye, Y. Yang, Z. Hong Hang, C. Qiu, and Z. Liu, Appl. Phys. Lett. **111**, 251107 (2017).
[15] F. Gao, H. Xue, Z. Yang, K. Lai, Y. Yu, X. Lin, Y. Chong, G. Shvets, and B. Zhang, Nat. Phys. **14**, 140 (2017).
[16] Z. Gao, Z. Yang, F. Gao, H. Xue, Y. Yang, J. Dong, and B. Zhang, Phys. Rev. B **96**, 201402(R) (2017).
[17] X. Wu, Y. Meng, J. Tian, Y. Huang, H. Xiang, D. Han, and W. Wen, Nat. Commun. **8**, 1304 (2017).
[18] J. Noh, S. Huang, K. P. Chen, and M. C. Rechtsman, Phys. Rev. Lett. **120**, 063902 (2018).

[19] F. D. M. Haldane and S. Raghu, Phys. Rev. Lett. **100**, 013904 (2008).
[20] Z. Wang, Y. D. Chong, J. D. Joannopoulos, and M. Soljacic, Phys. Rev. Lett. **100**, 013905 (2008).
[21] Z. Wang, Y. Chong, J. D. Joannopoulos, and M. Soljacic, Nature (London) **461**, 772 (2009).
[22] M. Hafezi, E. A. Demler, M. D. Lukin, and J. M. Taylor, Nat. Phys. **7**, 907 (2011).
[23] M. Hafezi, S. Mittal, J. Fan, A. Migdall, and J. M. Taylor, Nat. Photonics **7**, 1001 (2013).
[24] A. B. Khanikaev, S. H. Mousavi, W. K. Tse, M. Kargarian, A. H. MacDonald, and G. Shvets, Nat. Mater. **12**, 233 (2013).
[25] Y. Yang, Y. Poo, R.-x. Wu, Y. Gu, and P. Chen, Appl. Phys. Lett. **102**, 231113 (2013).
[26] M. C. Rechtsman, J. M. Zeuner, Y. Plotnik, Y. Lumer, D. Podolsky, F. Dreisow, S. Nolte, M. Segev, and A. Szameit, Nature (London) **496**, 196 (2013).
[27] W. J. Chen, S. J. Jiang, X. D. Chen, B. Zhu, L. Zhou, J. W. Dong, and C. T. Chan, Nat. Commun. **5**, 5782 (2014).
[28] W. Gao, M. Lawrence, B. Yang, F. Liu, F. Fang, B. Beri, J. Li, and S. Zhang, Phys. Rev. Lett. **114**, 037402 (2015).
[29] W. J. Chen, M. Xiao, and C. T. Chan, Nat. Commun. **7**, 13038 (2016).
[30] X. Cheng, C. Jouvaud, X. Ni, S. H. Mousavi, A. Z. Genack, and A. B. Khanikaev, Nat. Mater. **15**, 542 (2016).
[31] F. Gao, Z. Gao, X. Shi, Z. Yang, X. Lin, H. Xu, J. D. Joannopoulos, M. Soljacic, H. Chen, L. Lu, Y. Chong, and B. Zhang, Nat. Commun. **7**, 11619 (2016).
[32] Y. Wu, C. Li, X. Y. Hu, Y. T. Ao, Y. F. Zhao, and Q. H. Gong, Adv. Opt. Mater. **5**, 1700357 (2017).
[33] Z. Song, H. Liu, N. Huang, and Z. Wang, J. Phys. D: Appl. Phys. **51**, 095108 (2018).
[34] C. Li, X. Hu, W. Gao, Y. Ao, S. Chu, H. Yang, and Q. Gong, Adv. Opt. Mater. **6**, 1701071 (2017).
[35] M. Qiu, Appl. Phys. Lett. **81**, 1163 (2002).
[36] M. Hammer and O. V. Ivanova, Opt. Quantum Electron. **41**, 267 (2009).
[37] See Supplemental Material at http://link.aps.org/supplemental/10.1103/PhysRevMaterials.2.122201 for details about performance of three-dimensional devices, and robustness of the topological edge states against different defects.
[38] S. Ratzsch, E. B. Kley, A. Tunnermann, and A. Szeghalmi, Nanotechnology **26**, 024003 (2015).
[39] C. Xiong, W. H. Pernice, J. H. Ngai, J. W. Reiner, D. Kumah, F. J. Walker, C. H. Ahn, and H. X. Tang, Nano Lett. **14**, 1419 (2014).
[40] P. Tang, A. L. Meier, D. J. Towner, and B. W. Wessels, Opt. Lett. **30**, 254 (2005).
[41] C. Neusel and G. A. Schneider, J. Mech. Phys. Solids **63**, 201 (2014).
[42] Y. Drezner, M. Nitzani, and S. Berger, Appl. Phys. Lett. **86**, 042906 (2005).
[43] Y. Watanabe, D. Sawamura, and M. Okano, Appl. Phys. Lett. **72**, 2415 (1998).
[44] P. T. Lin, Z. Liu, and B. W. Wessels, J. Opt. A: Pure Appl. Opt. **11**, 075005 (2009).
[45] *The Angular Momentum of Light*, edited by D. L. Andrews and M. Babiker (Cambridge University Press, Cambridge, 2012).
[46] L. Lu, J. D. Joannopoulos, and M. Soljačić, Nat. Photonics **8**, 821 (2014).
[47] R. S. K. Mong and V. Shivamoggi, Phys. Rev. B **83**, 125109 (2011).
[48] Y. Yang, H. Jiang, and Z. H. Hang, Sci. Rep. **8**, 1588 (2018).
[49] P. Lodahl, S. Mahmoodian, S. Stobbe, A. Rauschenbeutel, P. Schneeweiss, J. Volz, H. Pichler, and P. Zoller, Nature (London) **541**, 473 (2017).
[50] R. J. Coles, D. M. Price, J. E. Dixon, B. Royall, E. Clarke, P. Kok, M. S. Skolnick, A. M. Fox, and M. N. Makhonin, Nat. Commun. **7**, 11183 (2016).
[51] J. Petersen, J. Volz, and A. Rauschenbeutel, Science **346**, 67 (2014).
[52] I. J. Luxmoore, N. A. Wasley, A. J. Ramsay, A. C. T. Thijssen, R. Oulton, M. Hugues, S. Kasture, V. G. Achanta, A. M. Fox, and M. S. Skolnick, Phys. Rev. Lett. **110**, 037402 (2013).
[53] I. Sollner, S. Mahmoodian, S. L. Hansen, L. Midolo, A. Javadi, G. Kirsanske, T. Pregnolato, H. El-Ella, E. H. Lee, J. D. Song, S. Stobbe, and P. Lodahl, Nat. Nanotechnol. **10**, 775 (2015).